The Aeronautical Journal (2024), 1–20
doi:10.1017/aer.2024.70

RESEARCH ARTICLE

Key factors affecting overexpanded flow separation in design of large expansion ratio single expansion ramp nozzle

Y. Yu[1,2,3], T. Yu[1,2], Y. Mao[2], Y. Yang[1,2] and S. Liang[1,2]

[1]School of Aeronautics, Chongqing Jiaotong University, 400074, Chongqing, China
[2]The Green Aerotechnics Research Institute of Chongqing Jiaotong University, Chongqing Key Laboratory of Green Aviation Energy and Power, 401120, Chongqing, China
[3]Jiangsu Province Key Laboratory of Aerospace Power System, Nanjing University of Aeronautics and Astronautics, 210016, Nanjing, China
Corresponding author: Y. Yu; Email: yuyang227@vip.sina.com

Received: 7 October 2023; **Revised:** 23 July 2024; **Accepted:** 30 July 2024

Keywords: Large expansion ratio; Single expansion ramp nozzle; Overexpansion; Flow separation pattern

Abstract

With the development of overall design methodologies for hypersonic vehicles and their propulsion systems, nozzles should expand airflow in a short length and provide sufficient thrust. Therefore, the large expansion ratio single expansion ramp nozzle (LSERN) is widely used. The form of the overexpanded flow field in the nozzle is complex, under the conditions of nozzle start-up, low speed and low nozzle pressure ratio (NPR), thereby negatively influencing the entire propulsion system. Thus, the nozzle flow separation pattern and the key factors affecting the flow separation pattern also deserve considerable attention. In this study, the design of SERN is completed using the cubic curve design method, and the model is numerically simulated for specific operating conditions to study the flow separation patterns and the transition processes of different patterns. Furthermore, the key factors affecting the various flow separation patterns in the nozzle are investigated in detail. Results show that the LSERN in different NPRs appeared in two types of restricted shock separation (RSS) pattern and free shock separation (FSS) pattern, as well as their corresponding flow separation pattern transition processes. The initial expansion angle and the nozzle length affect the range of NPRs maintained by the FSS pattern. The initial expansion angle affects the pattern of flow separation, whereas the nozzle length remarkably influences the critical NPR during transition.

Nomenclature

c	nozzle initial expansion angle
dy/dx	nozzle trailing edge angle
FSS	free shock separation
H_t	nozzle throat height
k	turbulent kinetic energy
LSERN	large expansion ratio single expansion ramp nozzle
NPR	nozzle pressure ratio
P_b	back pressure
P_w	nozzle wall pressure
RANS	Reynolds-Averaged Navier-Stokes
RSS	restricted shock separation
RSS (ramp)	restricted shock separation with separation bubble forming on ramp
RSS (flap)	restricted shock separation with separation bubble forming on flap
SERN	single expansion ramp nozzle

x_L	nozzle length
y	nozzle height
ϵ	turbulent dissipation rate

1.0 Introduction

An air-breathing propulsion system can use the oxygen in the atmosphere to react directly with the fuel [1–3], thereby greatly reducing the take-off weight and cost of the aircraft [4]. The scramjet is widely recognised as an efficient propulsion system for achieving hypersonic flight within Earth's atmosphere [5]. Nozzles are the primary components of a scramjet that generate thrust and provide some lift and pitch moment. A single expansion ramp nozzle (SERN) is a highly integrated afterbody and nozzle arrangement for hypersonic vehicles. This nozzle type positively affects weight reduction [6] and reduces resistance and friction loss at the bottom of the nozzle [7]. SERN is an optimal exhaust system, considering the impact of various parameters on the aircraft propulsion system [8–10]. Although the design of SERN has an excellent thrust coefficient in hypersonic flight, the nozzle operates in a state of overexpansion during the transonic stage, resulting in flow separation, which drastically reduces the performance [11, 12].

Research on nozzles in the overexpansion state has mostly focused on performance optimisation and flow separation. For performance optimisation, Ridgway et al. [9] investigated how alterations in geometry and operational factors affect SERN performance parameters. Their research indicated that variations in the shape and angle of the ramp, as well as the exit area and flap shape, had a substantial impact on thrust. Lv et al. [13] employed a secondary injection method on the cowl to effectively enhance the performance of the SERN. Under a nozzle pressure ratio (NPR) of 10, substantially improved SERN performance was achieved. Srinivasan et al. [14] experimentally measured wall static pressure to estimate various performance parameters of the nozzle. Additionally, they employed Schlieren flow visualisation techniques to observe the flow separation phenomena induced by shock waves and the resulting shock-wave interactions inside the nozzle under different NPRs.

The initial studies on the overexpansion flow separation are mainly focused on the rocket nozzle. Free shock separation (FSS) and restricted shock separation (RSS) are two common separation patterns in nozzles [15, 16], with FSS being the predominant pattern. Similar FSS and RSS patterns are also present in SERN, and a separation pattern transition has also occurred during nozzle start-up and shutdown. Yu et al. [17] observed two restricted shock separation patterns through wind tunnel experiments, namely the RSS pattern of the separation bubble on the ramp (RSS (ramp)) and the RSS pattern of the separation bubble on the flap (RSS (flap)), as shown in Figure 1. The FSS pattern is an unstable flow field pattern that is difficult to capture in the experiment. The RSS and FSS separation patterns of SERN were also observed in the numerical simulation results by Mousavi et al. [18]. He et al. [19] studied experimentally the separation features of SERN under fixed nozzle pressure ratios (NPR). The results indicate that the flow field exhibits RSS (ramp) pattern under the three conditions. When the NPR is higher, no reattachment flow is observed downstream of the expansion ramp, that is, the flow field exhibits an FSS pattern.

In practical scramjet nozzle design, a curved expansion ramp profile is employed, often coupled with a high nozzle pressure ratio to maximise the scramjet's performance capabilities. This combination results in the formation of a large expansion ratio single expansion ramp nozzle (LSERN). For hypersonic vehicles, the engine exhaust system and aircraft should be designed integrally, and the exhaust system must satisfy more stringent geometric constraints. Classical theoretical design methods, such as maximum thrust design [20, 21] and minimum length design [22], are insufficient to satisfy the design requirements. The cubic curve nozzle design approach offers enhanced flexibility in shaping the nozzle profile. It allows for nozzle configuration by specifying parameters such as throat height, nozzle length, outlet height, initial expansion angle and outlet airflow angle. Furthermore, optimisation techniques can be employed to refine the design, leading to improved overall results.

The large expansion ratio nozzle suffers from flow separation during the ground test and engine start-up and shutdown processes. The flow separation pattern transition is accompanied by a drastic shift in

https://doi.org/10.1017/aer.2024.70 Published online by Cambridge University Press

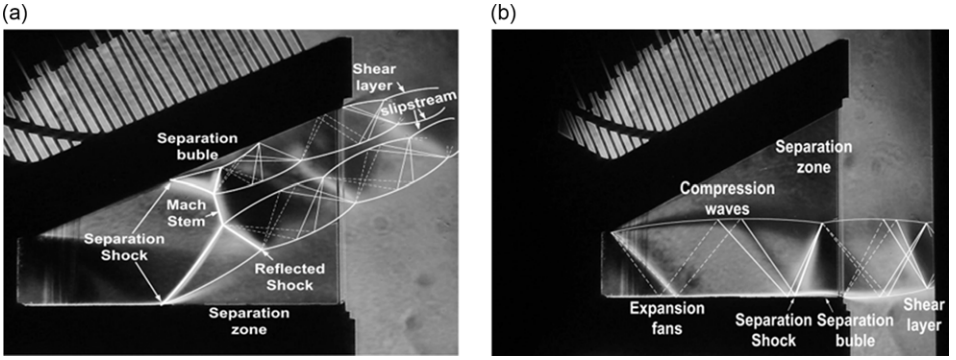

Figure 1. *Separation pattern in a straight expansion ramp SERN. (a) RSS (ramp) pattern, (b) RSS (flap) pattern.*

nozzle performance, which is a very dangerous situation if it occurs during engine operation, because it may endanger the flight safety of the vehicle and cause structural damage to the nozzle under extreme conditions. According to the referenced research findings [23], different flow separation patterns exist in the nozzle under different operating conditions, and the corresponding flow separation pattern transition occurs during the continuous change in conditions. The form of the overexpanded flow field in the nozzle is complex under the conditions of nozzle start-up, low speed and low NPR, thereby negatively influencing the entire propulsion system. Consequently, the flow separation pattern in the nozzle and the key factors affecting the flow separation pattern deserve considerable attention. Although the complex separation flow in the LSERN is one of the most important issues in the design of scramjet, researchers have not focused on this concept. Public studies have few experimental data and extensive flow characteristics analysis for the LSERN.

The present aims to extend the different flow separation flow field patterns found in the overexpansion state of the straight expansion ramp SERN and the corresponding flow separation pattern transition process to the large expansion ratio asymmetric thrust nozzle, as well as to discuss in detail the key factors affecting the overexpansion separation pattern of the LSERN. The performance of the system is predominantly influenced by the nozzle's geometry [24], and it also affects the flow separation pattern [25]. In this study, the LSERN designed by the cubic curve method is considered for investigation because it has a larger expansion ratio, and the nozzle design is more flexible. For the LSERN, essential design parameters encompass throat height, nozzle length, outlet height, initial expansion angle, and nozzle trailing edge angle. Subsequent sections will delve into the influence of nozzle pressure ratio, external Mach number, initial expansion angle and nozzle length on different separation patterns.

2.0 Numerical methods and models

2.1 Numerical method and validation

In simulating supersonic and hypersonic flows, high-resolution methods such as Direct Numerical Simulation (DNS) and Large Eddy Simulation (LES) are typically prioritised due to their capability to accurately capture flow details and transition phenomena [26, 27]. In contrast, the Reynolds-Averaged Navier-Stokes (RANS) method filters flow scales, including any transition and turbulent structures, through temporal averaging. Consequently, RANS is unable to precisely resolve the detailed structures of turbulence and transition phenomena and relies on empirical constants and assumptions, which may not universally apply across all flow scenarios. Despite the advantages of high-resolution methods like DNS and LES in accurately capturing flow details, given the superior computational efficiency and engineering applicability of RANS methods [28, 29], this study opts for RANS as the numerical approach. We have adopted the RNG k-ϵ turbulence model to simulate turbulent flow patterns [30, 31]. Within this model, turbulence is decomposed into two distinct equations, each representing the variations in

https://doi.org/10.1017/aer.2024.70 Published online by Cambridge University Press

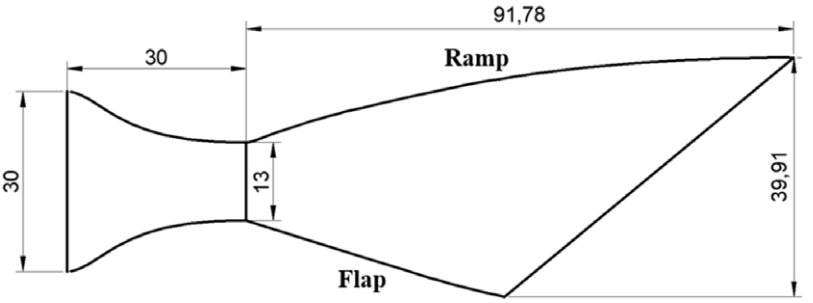

Figure 2. *Sketch of the SERN model.*

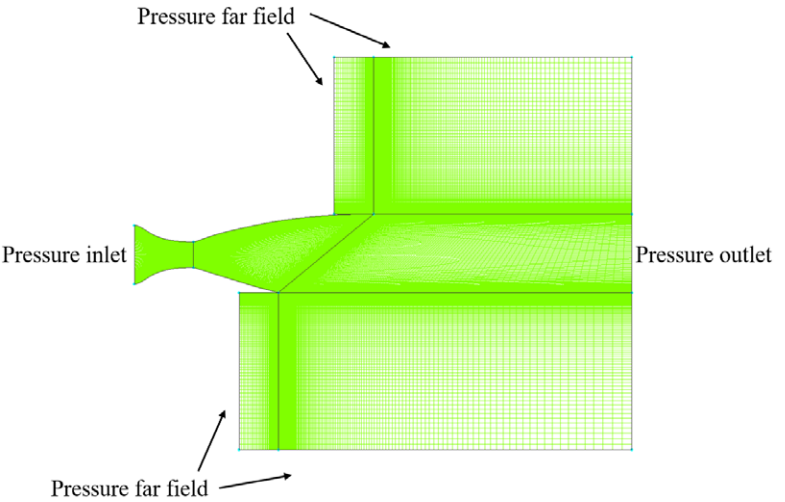

Figure 3. *Mesh of the SERN for numerical simulation.*

turbulent kinetic energy (k) and turbulent dissipation rate (ϵ). The k-ϵ model estimates turbulence characteristics by solving these two equations, including the distribution of turbulent kinetic energy and the intensity of turbulence [32, 33].

Before addressing the specific flow problem, the numerical simulation method must be verified using accurate experimental results. Figures 2 and 3 show the nozzle model and mesh for the numerical calculation, respectively. In this study, we refined the mesh in the nozzle expansion section to capture critical flow details. The $y+$ values used in the simulations were approximately 30, ensuring proper modeling within the boundary layer. The boundary conditions for the numerical calculations are consistent with those in Ref. (23), with a NPR of 3.5. The inlet total pressure is 124,008.5 Pa, and the static temperature is 296.5 K. The far field pressure is 35,422.69 Pa with a Mach number of 0 and a static temperature of 296.5 K. The outlet pressure is 35,422.69 Pa, and the static temperature is 296.5 K. The wall uses a no-slip boundary condition. Three different mesh resolutions were used for grid independence verification: coarse case (21,522), medium case (87,637) and fine case (353,667). These were compared with the experimental data from Ref. (23), as shown in Fig. 4. The results indicate that satisfactory calculation accuracy can be achieved using a medium resolution mesh. Consequently, the numerical simulation was conducted using the medium resolution mesh.

https://doi.org/10.1017/aer.2024.70 Published online by Cambridge University Press

Table 1. *Design conditions of cubic curve nozzle*

Design nozzle pressure ratio	Throat height	Specific heat ratio	Flap length	Outlet height
65	100 mm	1.3	100%	714.5 mm

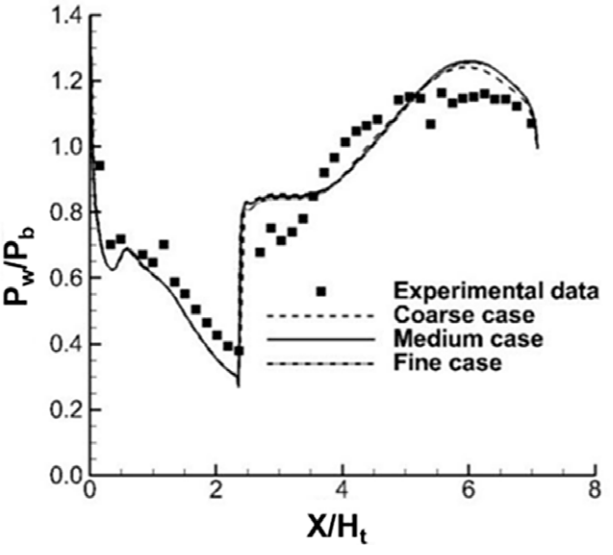

Figure 4. *Pressure distribution of ramp.*

2.2 Nozzle design method

The equation for the cubic curve profile of the nozzle is as follows:

$$y = ax^3 + bx^2 + cx + H_t \tag{1}$$

Where H_t is the throat height of the nozzle.

Derivation of Equation (1):

$$dy/dx = 3ax^2 + 2bx + c \tag{2}$$

When x=0,

$$dy/dx = c \tag{3}$$

Thus, c is the initial expansion angle of the nozzle.

When x=x_L, x_L is the length of the nozzle,

$$dy/dx = 3ax_L^2 + 2bx_L + c \tag{4}$$

is the trailing edge angle of the nozzle;

$$y = ax_L^3 + bx_L^2 + cx_L + H_t \tag{5}$$

is the nozzle height.

When designing the nozzle, given the initial expansion angle, trailing edge angle, nozzle length and nozzle outlet height, the parameters of a, b and c can be solved by Equations (3), (4) and (5), respectively. Table 1 and Fig. 5 show the nozzle design conditions and the nozzle profile design results, respectively. The contraction section of the nozzle is designed by the Vickers curve. The trailing edge angle is 0°, the initial expansion angle is 20°, and the length of the nozzle is 1,317.5 mm.

https://doi.org/10.1017/aer.2024.70 Published online by Cambridge University Press

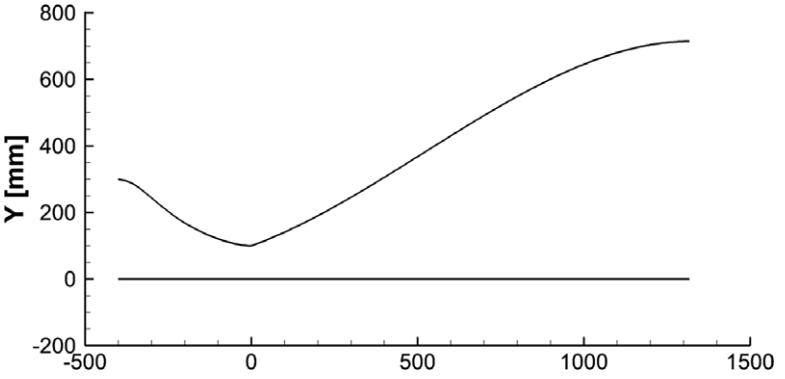

Figure 5. *Results of cubic curve design nozzle.*

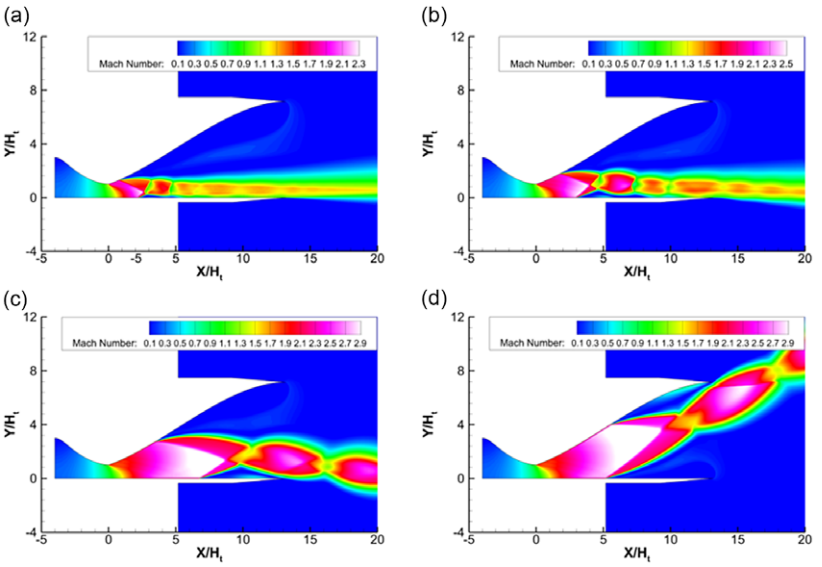

Figure 6. *Mach number contour at different nozzle pressure ratios for large expansion ratio SERN. (a) NPR = 3, (b) NPR = 4, (c) NPR = 8, (d) NPR = 10.*

3.0 Results and discussion

3.1 Flow separation pattern in LSERN

The effect of NPR on the flow separation pattern of LSERN is discussed. Figure 6 shows the Mach number contours of the flow field at various NPRs for a LSERN. The figure clearly shows that the nozzle can appear in the RSS (flap) pattern (Fig. 6(c)) and RSS (ramp) pattern (Fig. 6(d)) in the ground experimental state. Contrary to the model discussed in Ref. (25), the separated flow field in this LSERN has its own unique characteristics. The higher design NPR leads to an increase in both the inlet and outlet area ratios of the nozzle as well as the nozzle's length. In the case of the RSS (flap) pattern, the recirculation zone within the flap action range becomes more prominent and expansive within the flow field. Furthermore, the separation shock originating from the ramp is more noticeably pronounced, extending rearward and away from the throat. In addition, the airflow direction in front of the ramp separation shock varies at various nozzle pressure ratios due to the curved form of the nozzle ramp. When the airflow angle in front of the separation shock wave is large, directly modifying the jet to the

https://doi.org/10.1017/aer.2024.70 Published online by Cambridge University Press

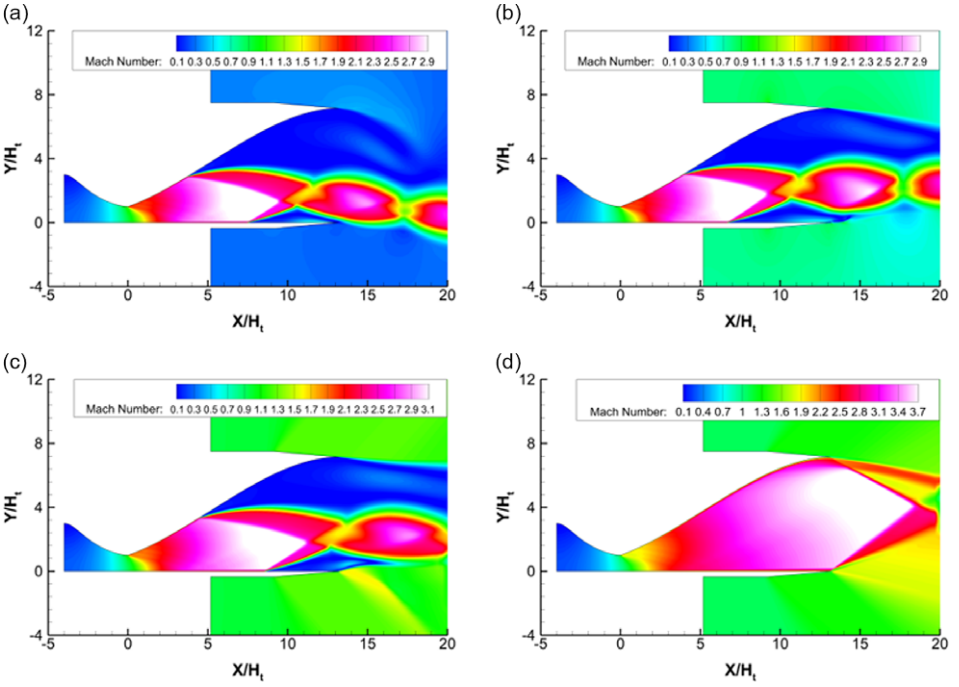

Figure 7. *Mach number contours at various external Mach numbers for NPR = 8. (a) Ma = 0.3, (b) Ma = 0.7, (c) Ma = 1.0, (d) Ma = 1.1.*

flap by one shock wave is difficult, as shown in Fig. 6(b). Consequently, a wide range of separation bubbles form in the flap.

Then, the effect of the external Mach number on the separation pattern is discussed. The recirculation zone generated by the ramp and flap in the overexpanded flow field is large due to the relatively high design NPR of the nozzle. When the external gas has a certain velocity, it can aggressively interact with the airflow in the recirculation zone, thereby affecting the flow field in the nozzle. Figure 7 shows the Mach number contours of the flow field in the nozzle at various external Mach numbers when the NPR=8. In a stationary external flow field, the flow pattern inside the nozzle transitions to the RSS (flap) configuration at NPR=8. As the external Mach number of the nozzle increases, the nozzle jet gradually deflected upward, the nozzle jet does not reattach to the flap, and the nozzle internal flow field transitioned to an FSS pattern, as shown in Fig. 4(b) and (c). With the further increase in the external Mach number, the separation shock wave disappears, a trailing edge shock is formed at the trailing edge, and the flow separation no longer occurs in the nozzle, as shown in Fig. 7(d). According to the discussion in Ref. (34), the external Mach number changes the nozzle flow field transitions from RSS to FSS pattern and finally to a situation where almost no separation is observed in the nozzle. Nevertheless, in the model presented in Ref. (34), the oblique shock wave persists inside the nozzle, and a small recirculation zone continues to exist after the separation shock wave. In contrast, the oblique shock wave within the proposed LSERN moves directly towards the nozzle's trailing edge, a phenomenon influenced by the angle of the nozzle's trailing edge.

At NPR=10, the flow field exhibits the RSS (ramp) pattern. Figure 8 illustrates Mach number contours within the nozzle for various external Mach numbers. At lower external Mach numbers, the outflow field's impact on the nozzle's mainstream remains limited, preserving the RSS (ramp) pattern, as depicted in Fig. 8(a). However, as the external Mach number increases, the flow field transitions to the FSS pattern, evident in Fig. 8(a) and (b). Subsequently, a trailing edge shock wave forms, eliminating airflow separation within the nozzle, as illustrated in Fig. 8(d).

https://doi.org/10.1017/aer.2024.70 Published online by Cambridge University Press

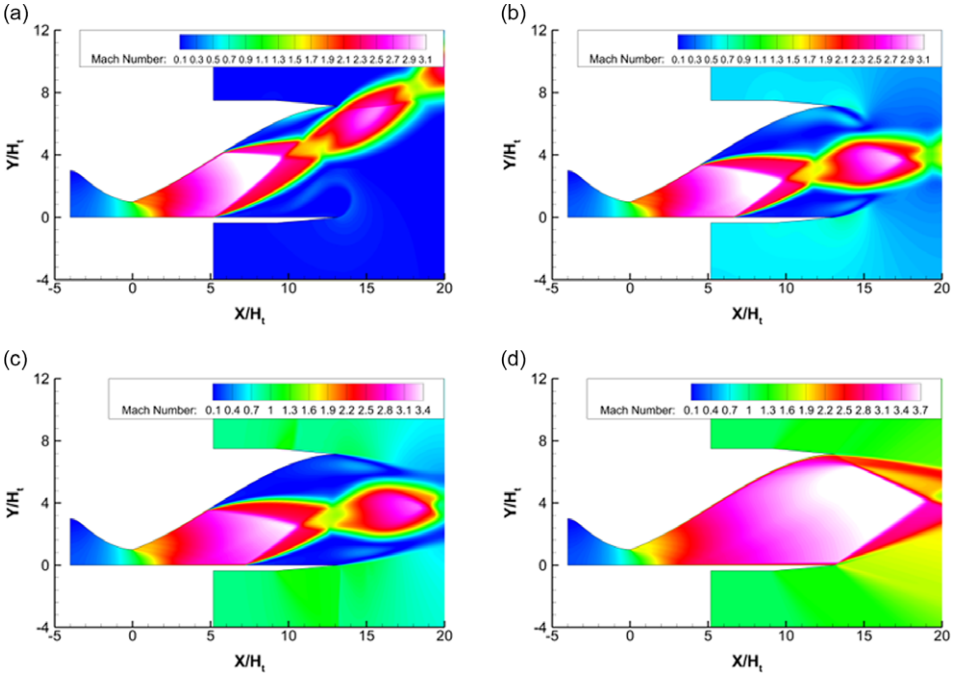

Figure 8. *Mach number contours at various external Mach numbers for NPR = 10. (a) Ma = 0.1, (b) Ma = 0.5, (c) Ma = 0.8, (d) Ma = 1.1.*

When the nozzle is in a state of overexpansion, its internal pressure falls below the ambient pressure. Figures 7 and 8 illustrate whether the nozzle is configured in the RSS (flap) or RSS (ramp) pattern. With the increase in the external Mach number, the transition to the FSS pattern is completed, eventually forming a flow field structure without separation. Whether flowing along the flap (RSS (flap) pattern) or along the ramp (RSS (ramp) pattern), the ambient gas drives the jet to deflect inside the nozzle. As the external Mach number increases, the momentum of the ambient gas increases, and the deflection of the jet becomes more evident. Finally, the jet cannot reattach on the wall, and the separation bubble on the wall is transformed into a recirculation zone connected to the environment. As the external Mach number increases further, the separation shock on the wall moves downstream, compressing the recirculation region. When the recirculation region on the wall can no longer be sustained, the separation shock moves towards the trailing edge, creating a trailing edge shock, and flow separation within the nozzle no longer occurs.

Although the initial flow fields of NPR 8 and 10 exhibit differences, as the external Mach number increases, both transition into the FSS pattern. However, upon careful observation, variations are noticeable in the resulting FSS pattern flow field. Specifically, differences in shock wave intensity emerge between the ramp and flap patterns, leading to distinct flow angles after the shock wave. As the flow field completes the RSS-FSS pattern transition, the relative intensity between the separation shock waves of the ramp and flap remains relatively constant. Following the RSS (flap) to FSS pattern transition, the ramp's separation shock wave exhibits higher intensity, effectively suppressing the development of the flap separation shock wave and limiting the recirculation zone on the flap, as depicted in Fig. 7c. Conversely, after the RSS (ramp) to FSS pattern transition, the flap separation shock wave maintains high intensity, resulting in a larger-scale recirculation zone formed by both the ramp and flap, as illustrated in Fig. 8c.

The preceding analysis highlights the diverse flow separation patterns observed in LSERN, with these patterns exhibiting variations in response to alterations in both the NPR and external Mach number. Notably, the NPR and external Mach number emerge as the predominant factors influencing flow

https://doi.org/10.1017/aer.2024.70 Published online by Cambridge University Press

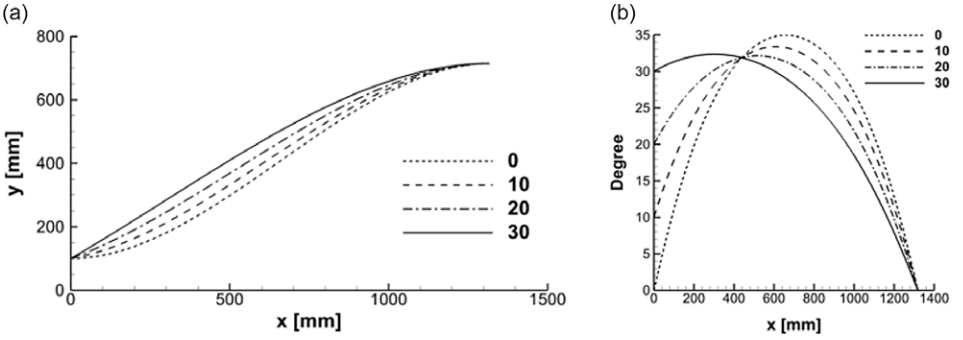

Figure 9. *Expansion ramp profile of the LSERN at varying initial expansion angles. (a) Expansion ramp profile, (b) Expansion ramp angle.*

separation patterns. Furthermore, it is worth noting that the initial flow separation configuration at the nozzle plays a pivotal role in shaping the subsequent transition process.

3.2 Effect of initial expansion angle on the flow separation pattern

The initial expansion angle is one of the most important parameters in the LSERN designed using the cubic curve method, because it directly affects the expansion of the airflow and the profile of the expansion ramp. Here, the nozzle design parameters are the same as those presented in Table 1. The effect of initial expansion angle, on the overexpansion flow field and the separation pattern is examined by varying its values. Figure 9 shows the initial expansion angle of 0°, 10°, 20° and 30° expansion ramp profiles. According to the results of the profile, as the initial expansion angle increases, the expansion ramp profile becomes steeper, and the angle at the trailing edge is adjusted to 0°.

Figure 10 shows the Mach number contours of the flow field inside the nozzle for various initial expansion angles of NPR = 4. In the given results, the flow fields are in the RSS (flap) pattern. When the initial expansion angle is less than 20°, the expansion ramp profile is relatively flat, and the airflow can be expanded to adhere to the ramp. Nonetheless, as the initial expansion angle increases, the expansion ramp profile gradually becomes steeper, the angle between the initial jet direction and the flap also gradually increases, the separation bubble of the flap gradually enlarges, and the flap of the separation shock wave in the flow field becomes increasingly apparent. Therefore, the airflow cannot be immediately deflected to flap the reattachment after passing through the ramp separation shock wave. When the initial expansion angle is 30°, due to the large deflection of the ramp at the throat, the airflow does not flow along the ramp, but is separated at the throat. The ramp does not appear to separate the shock wave because the airflow does not expand in the ramp; the airflow is not deflected by the shock wave, but by the influence of expansion waves and compression waves to deflect. Compression waves are reflected in the flap and gradually converge to form a separation shock and separation bubble; compression and expansion waves are formed to train downstream.

Figure 11 shows the Mach number contours of the flow field at various initial expansion angles for *NPR*=8. In the given results, the nozzles with initial expansion angles of 0°, 10° and 20° are in the RSS (flap) pattern, whereas the nozzle with initial expansion angle of 30° is in the RSS (ramp) pattern. An increase in NPR results in a backward shift of the separation shock waves at the ramp and flap when compared to the NPR=4 case. The separation bubble at the flap now forms right at the trailing edge, leading to airflow reattachment occurring precisely at the flap's trailing edge. In the RSS (flap) pattern with NPR=8, the Mach number before the ramp separation shock is approximately 2.5. The smaller initial expansion angle of the expansion ramp profile indicates that it is smoother near the throat. Furthermore, the increased length necessary to attain the separation Mach number, signifying a more rearward placement of the separation point, suggests that the separation shock associated with the ramp

https://doi.org/10.1017/aer.2024.70 Published online by Cambridge University Press

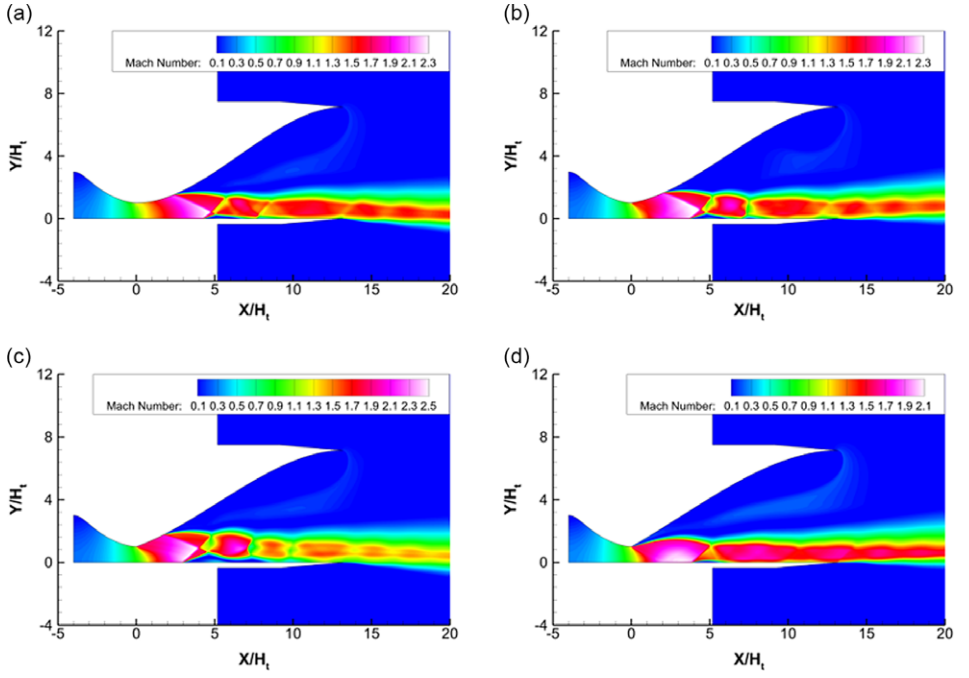

Figure 10. *Mach number contours of the flow field inside the nozzle for various initial expansion angles, NPR = 4. (a) Initial expansion angle of 0°, (b) Initial expansion angle of 10°, (c) Initial expansion angle of 20°, (d) Initial expansion angle of 30°.*

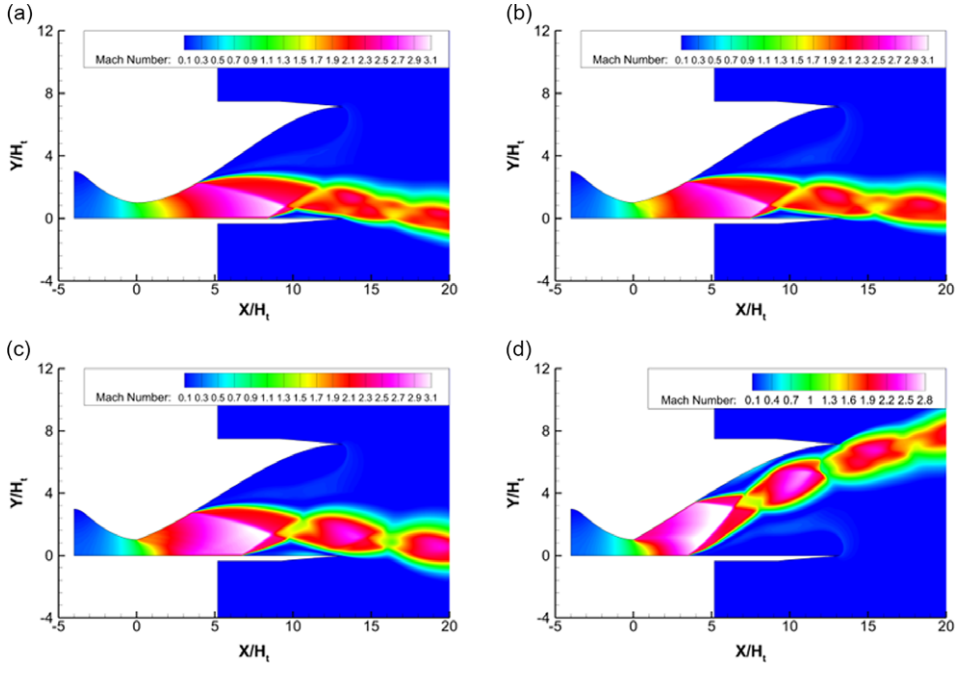

Figure 11. *Mach number contours of the flow field inside the nozzle for various initial expansion angles, NPR = 8. (a) Initial expansion angle of 0°, (b) Initial expansion angle of 10°, (c) Initial expansion angle of 20°, (d) Initial expansion angle of 30°.*

https://doi.org/10.1017/aer.2024.70 Published online by Cambridge University Press

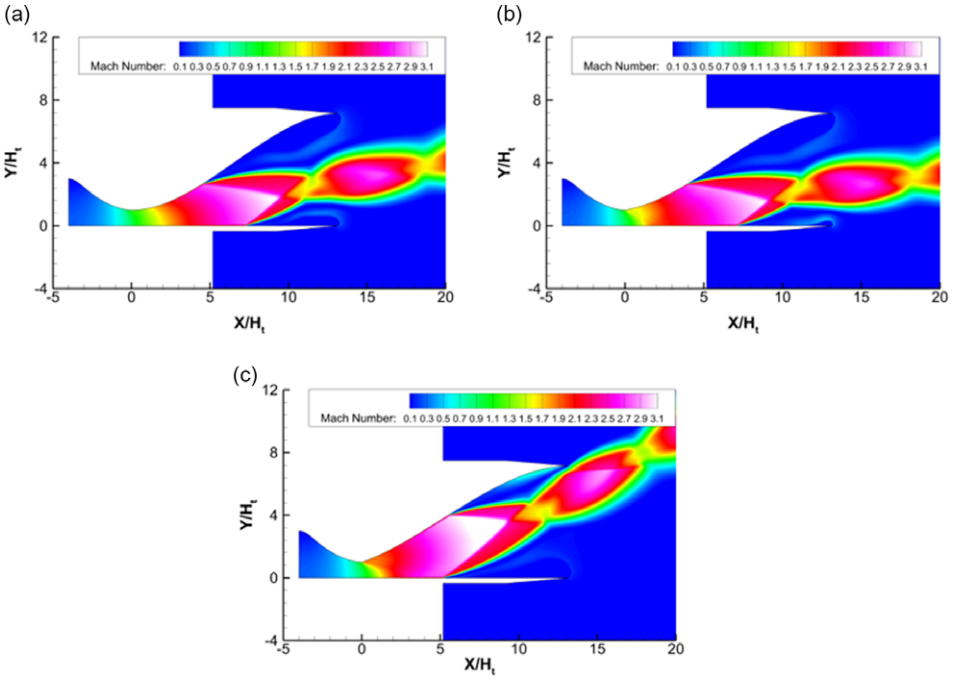

Figure 12. *Mach number contours of the flow field inside the nozzle for various initial expansion angles, NPR = 10. (a) Initial expansion angle of 0°, (b) Initial expansion angle of 10°, (c) Initial expansion angle of 20°.*

occurs closer to the trailing edge of the flap. This also results in a constrained scale for both the flap's separation bubble and its separation shock.

For the nozzle model with an initial expansion angle of 30°, the formation principle of the RSS (flap) pattern is different from that of the nozzles with initial expansion angles of 0°, 10° and 20°. The airflow does not expand on the ramp. When the NPR further increases, even if the airflow is still separated at the throat of the ramp, the jet boundary of the nozzle still gradually approaches the ramp until the airflow deflects to the ramp and continues to expand on the ramp. At this time, the flow angle of the ramp is larger, and the jet deflection through the ramp separation shock wave is insufficient to reattach it to the flap. Therefore, the RSS (flap) pattern cannot be maintained, and the flow field completes the transition from the RSS (flap) pattern to RSS (ramp) pattern.

Figure 12 displays Mach number contours for different initial expansion angles in a flow field with NPR=10. When compared to the NPR=8 results, the nozzles with 0° and 10° initial expansion angles shift from the RSS (flap) pattern to the FSS pattern. Meanwhile, the model with a 20° initial expansion angle transitions from the RSS (flap) pattern to the RSS (ramp) pattern. Figure 9(b) shows that when the initial expansion angle is 0° and 10°, the front profile of the expansion ramp is generally flat, but the airflow angle in the middle of the expansion ramp profile is large, and the change in the rear profile is relatively dramatic. At the NPR = 10, the location of the separation point on the ramp prior to the maximum position of the wall airflow angle and the separation shock wave after the expansion ramp profile slope continues to increase rapidly, causing the wall to move away from the jet rapidly. Consequently, the airflow cannot achieve reattachment on the ramp, resulting in the formation of an FSS pattern. For the initial expansion angle of 20°, the ramp separation point location in the wall airflow angle near the maximum position, not only after the separation shock wave angle is still large, and the expansion ramp profile slope rapidly decreases. The wall also begins to approach the jet, eventually achieving airflow separation and reattachment on the ramp, forming a typical RSS (ramp) pattern flow field. During the

https://doi.org/10.1017/aer.2024.70 Published online by Cambridge University Press

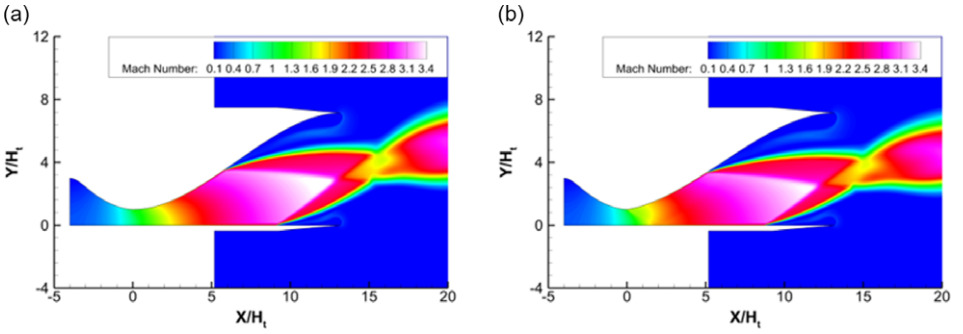

Figure 13. *Mach number contours of the flow field inside the nozzle for various initial expansion angles, NPR = 15. (a) Initial expansion angle of 0°, (b) Initial expansion angle of 10°.*

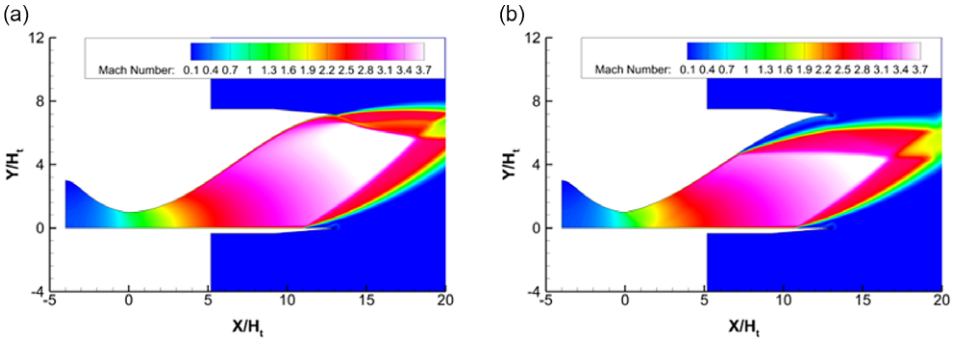

Figure 14. *Mach number contours of the flow field inside the nozzle for various initial expansion angles, NPR = 20. (a) Initial expansion angle of 0°, (b) Initial expansion angle of 10°.*

change in NPR, no stable FSS pattern flow field is found in the nozzle with initial expansion angles of 20° and 30°.

Figures 13 and 14 show the Mach number contours of the flow field for various initial expansion angles when NPR = 15 and NPR = 20, respectively. At this time, the flow field inside the nozzle is in the FSS pattern. As shown in Fig. 9(b), the rear slope of the expansion ramp profile changes drastically at initial expansion angles of 0° and 10°, reaching the outlet height rapidly in a shorter length. As a result, the jet cannot deflect toward the ramp, and the RSS (ramp) pattern cannot form. As the NPR continues to increase, the separation shock wave shifts backward and eventually forms the trailing edge shock wave.

The above analysis clearly indicates that the discussion of the design results for the cubic curve LSERN can be partially extended to other design methods as well. The initial expansion angle directly affects its expansion ramp profile. The expansion process of the jet on the wall is determined by the initial expansion angle. If the initial expansion angle is small, then the expansion ramp in the front of the nozzle is relatively flat, and in the rear of the nozzle changes dramatically, that is, the expansion at the throat is slower, whereas that in the rear of the nozzle is faster. Even if the NPR is relatively low at this stage, the airflow can still smoothly expand adhering to the ramp and form a separation shock wave at the ramp. Moreover, due to the relatively backward position of the separation point, the separation shock at the ramp is closer to the trailing edge, and the scale of the separation bubble in the RSS (flap) pattern is limited. The flow state in the RSS (flap) pattern is also easier to maintain. In addition, due to the large change in the slope of the expansion ramp profile at the rear of the nozzle, causing the rear of the nozzle profile to become steeper, achieving reattachment in the ramp is difficult, that is, the FSS

https://doi.org/10.1017/aer.2024.70 Published online by Cambridge University Press

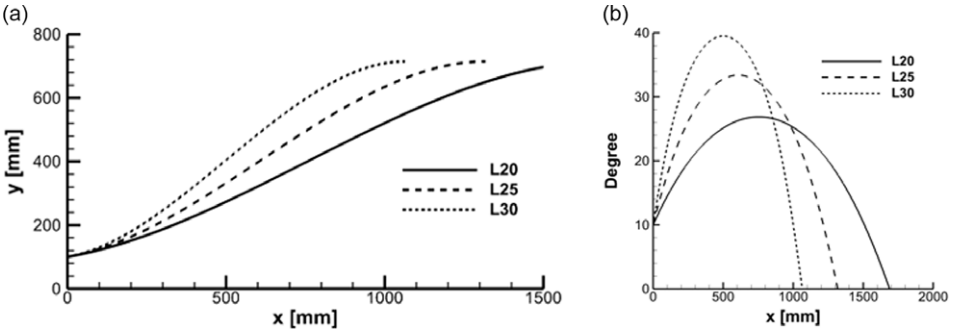

Figure 15. *Expansion ramp profile of the LSERN at various lengths with an initial expansion angle of 10°. (a) Expanded ramp profile, (b) Expansion ramp angle.*

pattern is also a relatively stable flow pattern, and the RSS (ramp) flow separation pattern is difficult to form. If the initial expansion angle is large, then the expansion ramp profile in front is steeper and slower in the rear; that is, the airflow expands fast after the throat and to a lesser extent in the rear. When the NPR is relatively low, the airflow cannot expand smoothly on the ramp, but rather separates at the throat; the ramp does not generate a separation shock wave. In this instance, the separation shock wave of the flap is not generated by the separation shock wave of the ramp, but rather by the reflection and convergence of the compression wave within the wave structure. When the NPR steadily increases, the jet boundary approaches the ramp, and the expansion on the ramp is ultimately realised, forming the RSS (ramp) pattern.

3.3 Effect of nozzle length on flow separation pattern

For this model, the initial expansion angle influences the distribution of the expansion process within the nozzle; the larger initial expansion angle, indicates faster airflow expansion in front of the nozzle and slower expansion at the rear. The nozzle length also affects the expansion process of the airflow. The longer nozzle length indicates smoother expansion of the airflow, whereas the larger space affects the formation and maintenance of the flow separation pattern. Figure 15 shows the expansion ramp profile of the LSERN at various lengths with an initial expansion angle of 10°. Maintaining the nozzle exit height constant, the length of the nozzle is the same as the length of the straight-walled nozzle with expansion angles of 20°, 25° and 30°, which is recorded as L20, L25 and L30. Figure 15 shows that, as the nozzle length increases, the maximum angle on the expansion ramp decreases, and the overall profile changes relatively smoothly.

Figure 15 shows the expansion ramp profile of the LSERN at various lengths with an initial expansion angle of 10°. The length of the nozzle is the same as the length of the straight-walled nozzle with expansion angles of 20°, 25° and 30°, which is recorded as L20, L25 and L30, respectively. Figure 15 shows that as the nozzle length increases, the maximum angle on the expansion ramp decreases and the overall profile changes relatively smoothly.

Figures 16, 17 and 18 show, the Mach number contours of typical NPRs for L20, L25 and L30 nozzles, respectively, with an initial expansion angle of 10°. During computations, the RSS (flap) and FSS pattern flow fields appear, but the NPRs for the transition from RSS (flap) to FSS pattern are different. The transition NPR for the L20 nozzle falls between 10 and 12; for the L25 nozzle, it falls between 8 and 10; for the L30 nozzle, it falls between 4 and 8.

Figure 19 shows the expansion ramp profile of the LSERN at various lengths with an initial expansion angle of 20°. Compared with the nozzle model with an initial expansion angle of 10°, the maximum angle of the expansion ramp has not changed substantially.

https://doi.org/10.1017/aer.2024.70 Published online by Cambridge University Press

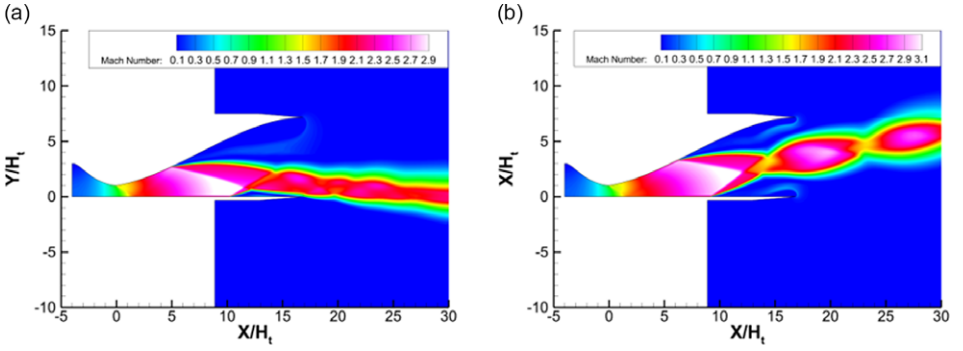

Figure 16. *Mach number contours for typical NPRs for L20 nozzle. (a) NPR=10, (b) NPR = 12.*

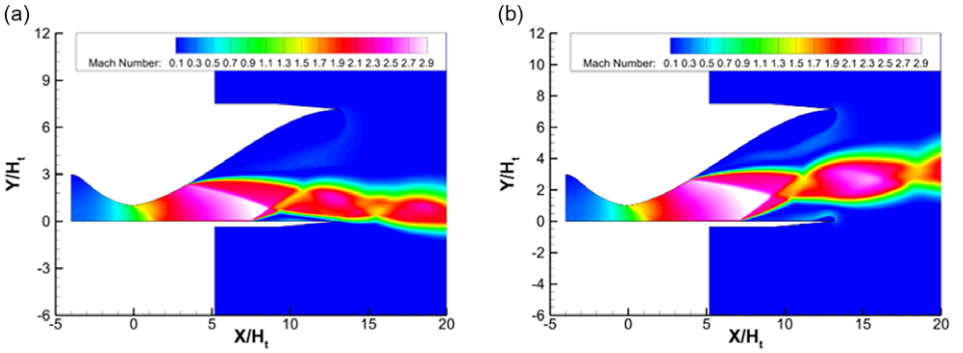

Figure 17. *Mach number contours for typical NPRs for L25 nozzle. (a) NPR=8, (b) NPR = 10.*

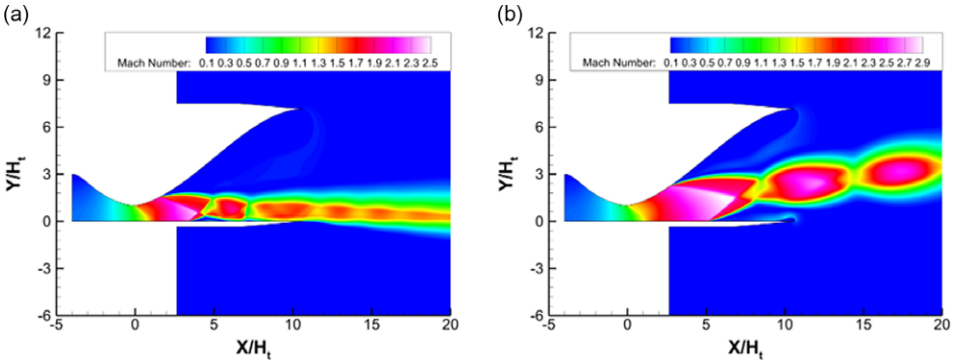

Figure 18. *Mach number contours for typical NPRs for L30 nozzle. (a) NPR = 4, (b) NPR = 8.*

Figures 20, 21 and 22 show the Mach number contours of NPRs for L20, L25 and L30 nozzles, respectively, with an initial expansion angle of 20°. During computations, the RSS (flap) and RSS (ramp) pattern flow fields appear, but the NPRs for the transition from RSS (flap) to RSS (ramp) pattern are different. The transition NPR for the L20 nozzle falls between 10 and 12; for the L25 nozzle, it falls between 8 and 10; for the L30 nozzle, it falls between 4 and 8.

Figure 23 shows the expansion ramp profile of the LSERN at various lengths with an initial expansion angle of 30°. Compared with the nozzle model with initial expansion angles of 10° and 20°, the maximum angle of the expansion ramp does not change significantly for the L25 and L30 nozzles. However, for the

https://doi.org/10.1017/aer.2024.70 Published online by Cambridge University Press

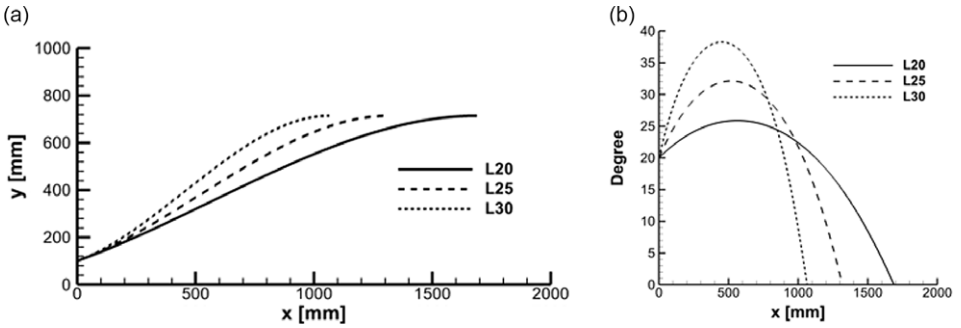

Figure 19. *Expansion ramp profile of the LSERN at various lengths with an initial expansion angle of 20°. (a) Expanded ramp profile, (b) Expansion ramp angle.*

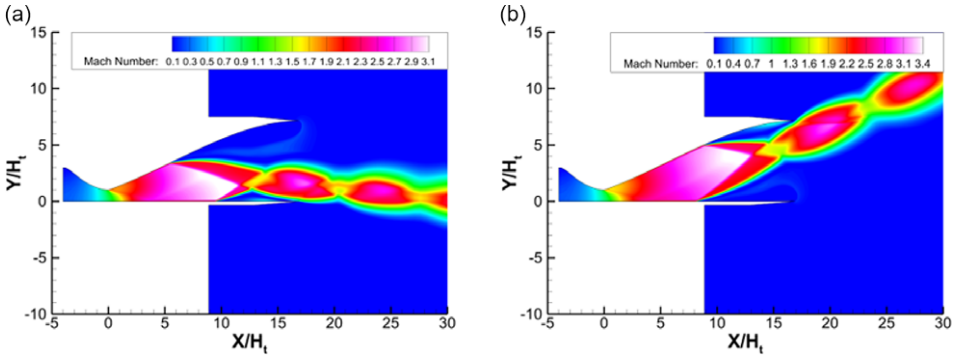

Figure 20. *Mach number contours for typical NPRs for L20 nozzle. (a) NPR = 10, (b) NPR = 12.*

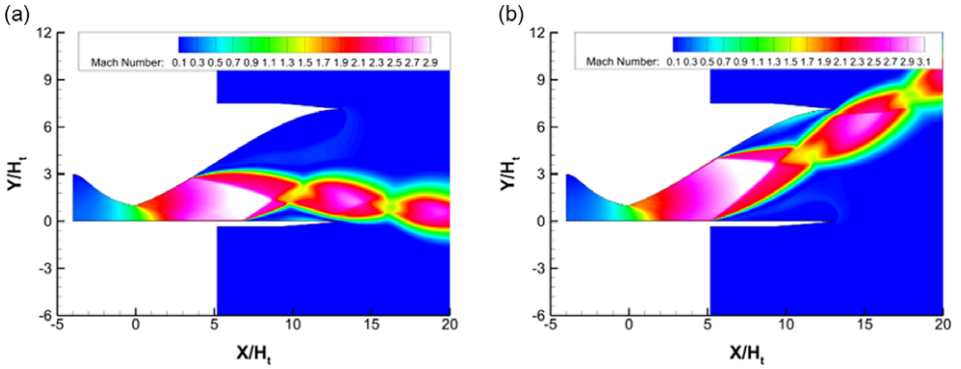

Figure 21. *Mach number contours for typical NPRs for L25 nozzle. (a) NPR = 8, (b) NPR = 10.*

expansion ramp of the L20 nozzle, the initial expansion angle of 30° is the maximum deflection angle on the expansion ramp. Then, the wall angle gradually decreases, forming a convex curve.

Figures 24, 25 and 26 show the Mach number contours of typical NPRs for L20, L25 and L30 nozzles, respectively, with an initial expansion angle of 20°. During computations, the RSS (flap) and RSS (ramp) pattern flow fields appear, but the NPRs for the transition from RSS (flap) to RSS (ramp) pattern are different. The transition NPR for the L20 nozzle falls between 8 and 10; for the L25 nozzle, it falls between 4 and 8; for the L30 nozzle, it falls between 4 and 8.

https://doi.org/10.1017/aer.2024.70 Published online by Cambridge University Press

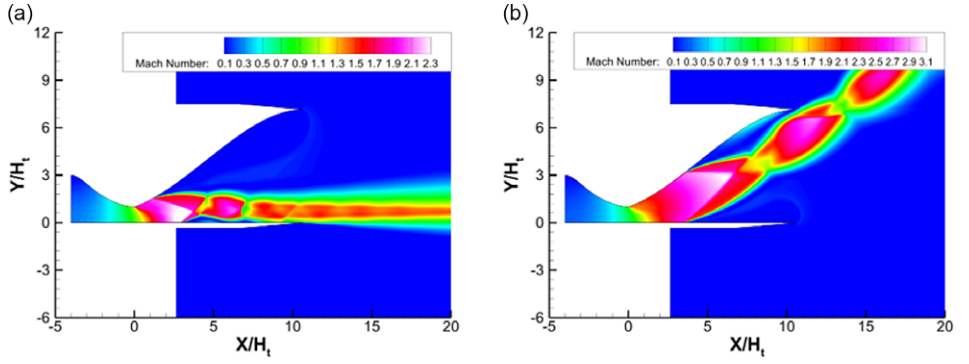

Figure 22. *Mach number contours for typical NPRs for L30 nozzle. (a) NPR = 4, (b) NPR = 8.*

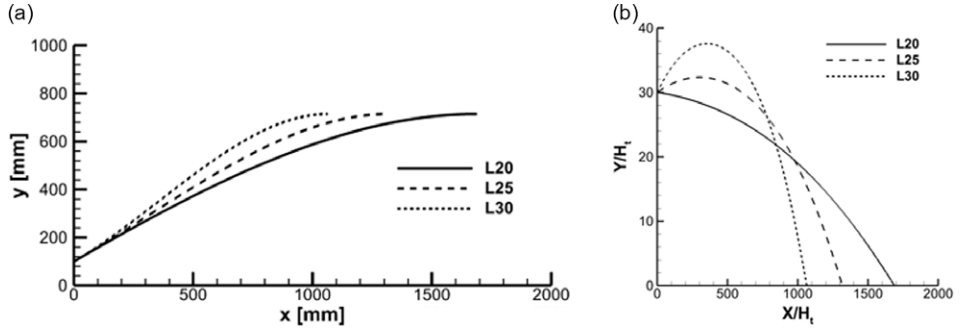

Figure 23. *Expansion ramp profile of the LSERN at various lengths with an initial expansion angle of 30°. (a) Expanded ramp profile, (b) Expansion ramp angle.*

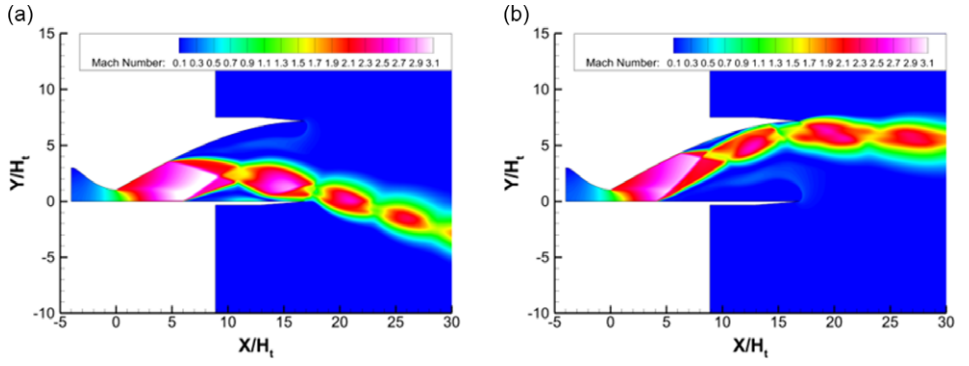

Figure 24. *Mach number contours for typical NPRs for L20 nozzle. (a) NPR = 8, (b) NPR = 10.*

Figure 27 gathers the separation patterns in the overexpanded LSERN obtained by numerical simulation for various cases in the full text. The figure evidently shows that, when the nozzle length is the same, for smaller initial expansion angles, the FSS pattern can be maintained over a larger range of NPRs. In addition, the longer length of the nozzle indicates greater range of NPRs that can be maintained by the FSS pattern. Under the same initial expansion angle conditions, the critical NPR for the separation pattern transition decreases as the nozzle length increases. However, the nozzle length does not affect the classification of separation pattern before and after the transitions. Based on the previous results, the

https://doi.org/10.1017/aer.2024.70 Published online by Cambridge University Press

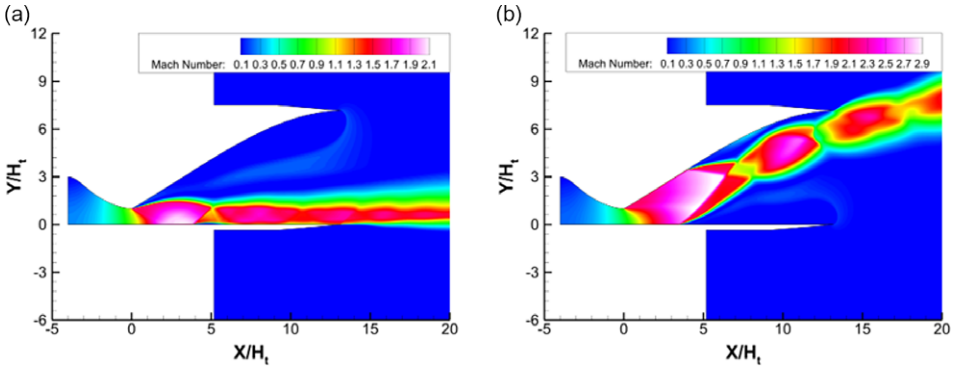

Figure 25. *Mach number contours for typical NPRs for L25 nozzle. (a) NPR = 4, (b) NPR = 8.*

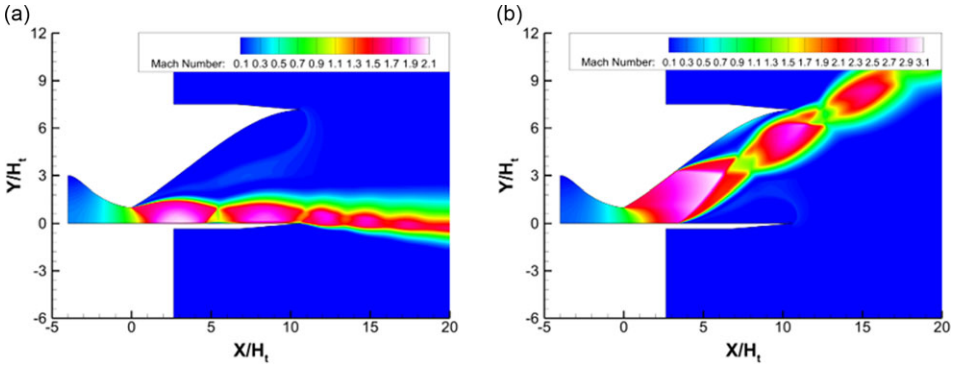

Figure 26. *Mach number contours for typical NPRs for L30 nozzle. (a) NPR = 4, (b) NPR = 8.*

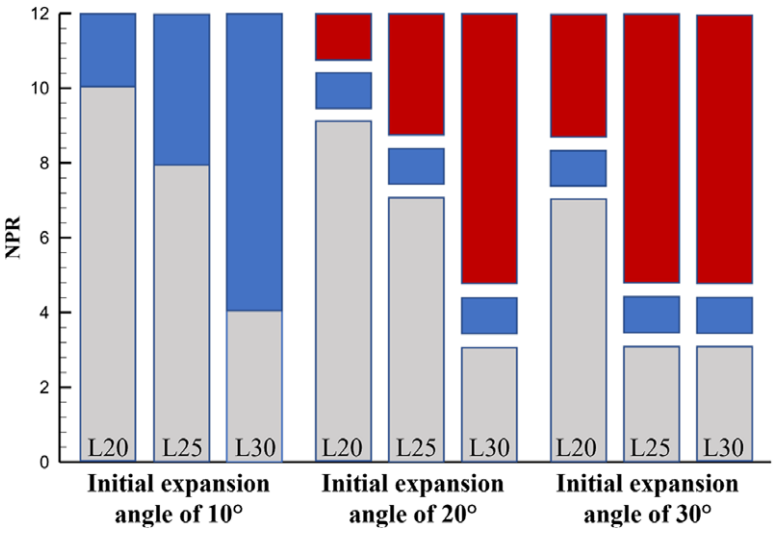

Figure 27. *Flow separation patterns in overexpanded LSERN with varying nozzle lengths and initial expansion angles; grey blocks indicate RSS (flap); blue blocks indicate FSS; red blocks indicate RSS (ramp).*

https://doi.org/10.1017/aer.2024.70 Published online by Cambridge University Press

initial expansion angle influences the flow separation pattern, but the nozzle length is more of a critical NPR that influences the transition of the flow separation pattern.

4.0 Conclusion

In this study, the various flow separation patterns found in the straight-walled SERN and the corresponding flow separation pattern translation process are extended to the large expansion ratio asymmetric thrust nozzle. In the numerical simulation of the LSERN, the same RSS (flap), RSS (ramp) and FSS flow separation patterns, as well as their corresponding flow separation pattern transitions were observed under various NPRs.

For the LSERN, the effect of external Mach number on the overexpansion flow field is more pronounced. Strong interactions are observed between the external gas and the recirculation zone of the flap as well as the boundary layer of the ramp. As the external flow Mach number increases, the flow field transitions from the RSS pattern to the FSS pattern, and eventually develops into a flow field pattern without flow separation in the nozzle.

In addition, a discussion of the key factors affecting the flow separation pattern reveals that the initial expansion angle directly affects the expansion ramp profile of the nozzle, which actually determines the expansion process of the jet on the wall of the nozzle. For different initial expansion angles of the nozzle model, the flow separation mode transition process caused by the NPR is also different. In the same NPR range, when the initial expansion angle is low, the transition from the RSS (flap) to FSS occurs, whereas when the initial expansion angle is large, the transition from the RSS (flap) to RSS (ramp) occurs. Thus, the initial expansion angle affects the flow separation pattern that occurs in the nozzle. When the nozzle length is the same, for smaller initial expansion angles, the FSS pattern can be maintained over a larger range of NPRs. In addition, the longer nozzle length indicates greater range of NPRs that can be maintained by the FSS pattern. Moreover, under the same initial expansion angle conditions, as the nozzle length increases, the critical NPR of the separation pattern transition decreases, but the nozzle length does not affect the final result of the flow separation pattern transition. Therefore, the initial expansion angle influences the flow separation pattern inside the nozzle, whereas the nozzle length remarkably affects the critical NPR when the transition occurs.

Acknowledgements. This work is supported by the Scientific and Technological Research Program of Chongqing Municipal Education Commission (Grant No. KJZD-M202100702), the China Space Foundation Aerospace Propulsion Public Welfare Special Fund (Grant No. KDJJ20230201006), the National Natural Science Foundation of China (Grant No. 11802124). The numerical calculations in this paper have been done on Hefei advanced computing center.

Competing interests. The authors declare that they have no competing interests.

References

[1] Bordoloi, N., Pandey, K.M., Ray, M. and Kumar Sharma, K. Computational investigation to interpret the reacting flow conditions for two different fuels in the scramjet combustor, *Results Eng.*, 2022, **15**, p 100568. https://doi.org/10.1016/j.rineng.2022.100568

[2] Jones, J.P., Kuffel, L., Sorto-Ramos, E., Seyed Alavi, K., Mccall, T. and Chudoba, B. Investigating the legacy of air-breathing and rocket propulsion systems, In AIAA Propulsion and Energy 2020 Forum (1–0). American Institute of Aeronautics and Astronautics, 2020. https://doi.org/10.2514/6.2020-3916

[3] Urzay, J. Supersonic combustion in air-breathing propulsion systems for hypersonic flight, *Annu. Rev. Fluid. Mech.*, 2018, **50**, (1), pp 593–627. https://doi.org/10.1146/annurev-fluid-122316-045217

[4] Baidya, R., Pesyridis, A. and Cooper, M. Ramjet nozzle analysis for transport aircraft configuration for sustained hypersonic flight, *Appl. Sci.*, 2018, **8**, (4), 574. https://doi.org/10.3390/app8040574

[5] Wang, J.P., Zhuo, C.F., Dai, C.L. and Sun, B. Numerical investigation of thermochemical non-equilibrium effects in Mach 10 scramjet nozzle, *Aeronaut. J.*, 2024, **First View**, 1–18. https://doi.org/10.1017/aer.2024.47

[6] Spoth, K. and Moses, P. Structural design and analysis of a Mach zero to five turbo-ramjet system, In *29th Joint Propulsion Conference and Exhibit (1–0). American Institute of Aeronautics and Astronautics,* 1993. https://doi.org/10.2514/6.1993-1983

https://doi.org/10.1017/aer.2024.70 Published online by Cambridge University Press

[7] Snyder, L., Escher, D., DeFrancesco, R., Gutierrez, J. and Buckwalter, D. Turbine Based Combination Cycle (TBCC) propulsion subsystem integration. In *40th AIAA/ASME/SAE/ASEE Joint Propulsion Conference and Exhibit (1–0)*. American Institute of Aeronautics and Astronautics, 2004. https://doi.org/10.2514/6.2004-3649

[8] Malla, B., Holder, J., Anand, V. and Gutmark, E. Structural excitation of SERNs during supersonic operation: A source of screech amplitude modulation, *J. Fluids Struct.*, 2021, **107**, p 103390. https://doi.org/10.1016/j.jfluidstructs.2021.103390

[9] Ridgway, A., Sam, A.A. and Pesyridis, A. Modelling a hypersonic single expansion ramp nozzle of a hypersonic aircraft through parametric studies, *Energies*, 2018, **11**, (12), p 3449. https://doi.org/10.3390/en11123449

[10] Zhou, L., Liu, Z., Wang, Z. and Xiao, H. Numerical study of passive cavity control on high-pressure ratio single expansion ramp nozzle under over-expansion condition. Proc. Inst. Mech. Eng. G J. Aerosp. Eng., 2016, 230, (8), pp 1409–1422. https://doi.org/10.1177/0954410015611152

[11] Hemmati, A. and Namazian, Z. Numerical analysis of shock wave train in single-expansion ramp nozzle under harmonic inlet and outlet conditions, *Chem. Eng. Commun.*, 2021, pp 1–10. https://doi.org/10.1080/00986445.2021.2007091

[12] Mirjalily, S.A.A. Calibration of the k-ω shear stress transport turbulence model for shock wave boundary layer interaction in a SERN using machine learning, *Eng. Anal. Bound. Elem.*, 2023, **146**, pp 96–104. https://doi.org/10.1016/j.enganabound.2022.10.009

[13] Lv, Z., Xu, J. and Mo, J. Numerical investigation of improving the performance of a single expansion ramp nozzle at off-design conditions by secondary injection, *Acta Astronaut.*, 2017, **133**, pp 233–243. https://doi.org/10.1016/j.actaastro.2017.01.013

[14] Srinivasan, P., Muruganandam, T.M. and Balusamy, K. Effect of flap deflection on single-expansion-ramp nozzles performance at different pressure ratios, *J. Propul. Power*, 2022, **38**, (6), pp 1025–1041. https://doi.org/10.2514/1.B38680

[15] Frey, M. and Hagemann, G. Flow separation and side-loads in rocket nozzles, In *35th Joint Propulsion Conference and Exhibit (1–0)*. American Institute of Aeronautics and Astronautics, 1999. https://doi.org/10.2514/6.1999-2815

[16] Nave, L. and Coffey, G. Sea level side loads in high-area-ratio rocket engines, In *9th Propulsion Conference (1–0)*. American Institute of Aeronautics and Astronautics, 1973. https://doi.org/10.2514/6.1973-1284

[17] Yu, Y., Xu, J., Yu, K. and Mo, J. Unsteady transitions of separation patterns in single expansion ramp nozzle, *Shock Waves*, 2015, **25**, (6), pp 623–633. https://doi.org/10.1007/s00193-015-0595-y

[18] Mousavi, S.M., Pourabidi, R. and Goshtasbi-Rad, E. Numerical investigation of over expanded flow behavior in a single expansion ramp nozzle, *Acta Astronaut.*, 2018, **146**, 273–281. https://doi.org/10.1016/j.actaastro.2018.03.003

[19] He, C., Li, J., Fan, Z., Li, Y., Liang, J., Miao, L. and Gao, R. Wall pressure unsteadiness in an over-expanded single expansion ramp nozzle, *Int. J. Modern Phys. B*, 2020, **34**, (14n16), p 2040102. https://doi.org/10.1142/S0217979220401025

[20] Lv, Z., Xu, J., Yu, Y. and Mo, J. A new design method of single expansion ramp nozzles under geometric constraints for scramjets, *Aerosp. Sci. Technol.*, 2017, **66**, pp 129–139. https://doi.org/10.1016/j.ast.2017.03.013

[21] Yu, K., Chen, Y., Huang, S., Lv, Z. and Xu, J. Optimization and analysis of inverse design method of maximum thrust scramjet nozzles, *Aerosp. Sci. Technol.*, 2020, **105**, p 105948. https://doi.org/10.1016/j.ast.2020.105948

[22] Zebbiche, T. Stagnation pressure effect on the supersonic minimum length nozzle design, *Aeronaut. J.*, 2019, **123**, (1265), pp 1013–1031. https://doi.org/10.1017/aer.2019.42

[23] Yu, Y., Xu, J., Mo, J. and Wang, M. Numerical investigation of separation pattern and separation pattern transition in overexpanded single expansion ramp nozzle, *Aeronaut. J.*, 2014a, **118**, (1202), pp 399–424. https://doi.org/10.1017/S0001924000009192

[24] Yu, Y., Shademan, M., Barron, R.M. and Balachandar, R. CFD study of effects of geometry variations on flow in a nozzle, *Eng. Appl. Comput. Fluid Mech.*, 2012, **6**, (3), 412–425. https://doi.org/10.1080/19942060.2012.11015432

[25] Yu, Y., Xu, J., Mo, J. and Wang, M. Principal parameters in flow separation patterns of over-expanded single expansion RAMP nozzle, *Eng. Appl. Comput. Fluid Mech.*, 2014b, **8**(2), pp 274–288. https://doi.org/10.1080/19942060.2014.11015513

[26] Drikakis, D., Ritos, K., Spottswood, S.M. and Riley, Z.B. Flow transition to turbulence and induced acoustics at Mach 6, *Phys Fluids (1994)*, 2021, **33**, (7), p 076112. https://doi.org/10.1063/5.0054345

[27] Kokkinakis, I.W., Drikakis, D., Ritos, K. and Spottswood, S.M. Direct numerical simulation of supersonic flow and acoustics over a compression ramp, *Phys Fluids (1994)*, 2020, **32**, (6), p 066107. https://doi.org/10.1063/5.0010548

[28] Yu, T., Wu, X., Yu, Y., Li, R. and Zhang, H. Establishment and validation of a relationship model between nozzle experiments and CFD results based on convolutional neural network, *Aerosp. Sci. Technol.*, 2023, **142**, p 108694. https://doi.org/10.1016/j.ast.2023.108694

[29] Yu, T., Yu, Y., Mao, Y.P., Yang, Y.L. and Xu, S.L. Comparative study of OpenFOAM solvers on separation pattern and separation pattern transition in overexpanded single expansion ramp nozzle, *J. Appl. Fluid Mech.*, 2023, **16**, (11), pp 2249–2262. https://doi.org/10.47176/jafm.16.11.1751

[30] Jia, S., Cao, X., Wang, F., Zhang, C., Yuan, X. and Yu, K.-T. Renormalization group method for the turbulent mass transport two-equation model, *Chem. Eng. Sci.*, 2022, **249**, p 117306. https://doi.org/10.1016/j.ces.2021.117306

[31] Li, Y., Zhou, Y., Xiao, Y. and Yang, W. Study of gas-solid two-phase flow in pipeline elbows using an LES-DPM coupling method, *Powder Technol.*, 2023, **413**, p 118012. https://doi.org/10.1016/j.powtec.2022.118012

[32] Galván, S., Reggio, M. and Guibault, F. Assessment study of K-ε turbulence models and near-wall modeling for steady state swirling flow analysis in draft tube using fluent, *Eng. Appl. Comput. Fluid Mech.*, 2011, **5**, (4), pp 459–478. https://doi.org/10.1080/19942060.2011.11015386

https://doi.org/10.1017/aer.2024.70 Published online by Cambridge University Press

[33] Rahimzadeh, H., Maghsoodi, R., Sarkardeh, H. and Tavakkol, S. Simulating flow over circular spillways by using different turbulence models, *Eng. Appl. Comput. Fluid Mech.*, 2012, **6**, (1), pp 100–109. https://doi.org/10.1080/19942060.2012.11015406

[34] Yu, Y. Over-expanded separation transitions of single expansion ramp nozzle in the accelerating and decelerating processes, *Aerosp. Sci. Technol.*, 2020, **98**, p 105674. https://doi.org/10.1016/j.ast.2019.105674

Cite this article: Yu Y., Yu T., Mao Y., Yang Y. and Liang S. Key factors affecting overexpanded flow separation in design of large expansion ratio single expansion ramp nozzle. *The Aeronautical Journal*, https://doi.org/10.1017/aer.2024.70